Journal of Nuclear Materials 582 (2023) 154466

Contents lists available at ScienceDirect

Journal of Nuclear Materials

journal homepage: www.elsevier.com/locate/jnucmat

Nitriding model for zirconium based fuel cladding in severe accident codes

B.S. Jäckel [a,c], J.C. Birchley [a,c], T. Lind [a,*], M. Steinbrück [b], S. Park [a,1]

[a] Paul Scherrer Institute, Switzerland, UK
[b] Karlsruhe Institute of Technology, Germany
[c] Retired, Switzerland, UK

HIGHLIGHTS

- Model developed for reactions of nitrogen during air oxidation of Zr-cladding.
- Data from separate effect tests used to develop the model.
- Decisive importance of α-Zr(O) for nitriding reaction.
- Model implemented in special version of MELCOR 1.8.6 for simulation of air ingress sequences in reactors and spent fuel pools.

ARTICLE INFO

Keywords:
Cladding
Air ingress
Air oxidation
Nitriding

ABSTRACT

A model has been developed to describe the nitriding of partially oxidized zirconium based cladding during an air ingress sequence when the reaction has become starved of oxidant (oxygen and/or steam), and the subsequent re-oxidation of nitride following of restoration of coolant. Key aspects of the model are the estimation of oxygen-stabilised alpha zirconium, α-Zr(O), formed during pre-oxidation and its reaction with the nitrogen. Nitriding of metallic Zr is much slower than α-Zr(O), and plays a comparatively minor role. The model is based on data from separate-effects tests comprised pre-oxidation, nitriding in the absence of oxidant, and re-oxidation in the absence of nitrogen, which were used to derive the kinetic parameters for the main reaction processes. Developmental assessment was performed using the test results, demonstrating favourable agreement for the main reaction signatures. Independent assessment against Integral Test data is underway.

1. Introduction

One of the potential impacts of air ingress to overheated fuel during a reactor or spent fuel accident is the formation of zirconium nitride (ZrN). The reaction is not only a source of heat, but the ZrN itself reacts readily and exothermically with oxygen, steam or even liquid water, with the release of nitrogen. The formation of nitride, even in trace amounts, causes the oxide layer to lose its effectiveness as a protective layer to limit further oxidation.

Concerns over the risks of air ingress was first raised by Powers et al. [1] following the realisation that the TMI-2 reactor vessel had been worryingly close to lower head failure [2]. If the vessel had failed, there would have been a pathway for air to ingress into the already severely damaged core. Air oxidation kinetics were the subject of debate and experimental studies [3]. The main concerns at the time were the effect of accelerated kinetics on the ongoing accident escalation, and the risk that exposure of the fuel itself to oxygen would render certain of the radiotoxic actinides and fission products in a more volatile state.

Further attention was focussed on air ingress sequence following the Paks cleaning tank incident in 2003 [4]. Several experimental programs were launched to investigate the impacts and to characterise the chemical-dynamic processes in order to enable analysis and risks assessments of the associated threats. Separate-effects test (SET) programs to furnish basic data were launched at IRSN, France [5] and KIT, Germany [6,7]. The integral test programs include QUENCH (KIT, Karlsruhe, Germany) [8], PARAMETER SF4 (Luch, Russia) [9], CODEX AIT (AEKI, Hungary) [10], and the SFP-1 and −2 (Sandia National Labs, USA) [11]. The main issue regarding core damage escalation was hitherto considered to be the accelerated oxidation kinetics due to the effect of nitrogen on the integrity of the oxide layer. However, several of the

* Corresponding author.
E-mail address: terttaliisa.lind@psi.ch (T. Lind).
[1] Present affiliation: Lee and Co., South Korea.

https://doi.org/10.1016/j.jnucmat.2023.154466
Received 5 January 2023; Received in revised form 29 March 2023; Accepted 18 April 2023
Available online 21 April 2023

integral tests demonstrated very significant nitriding and major impacts on subsequent coolability.

In particular, the QUENCH-16 [12] and QUENCH-18 [13] experiments, with air oxidation under starvation of oxidant, yielded data which showed extensive formation of zirconium nitride followed by strongly enhanced hydrogen production during the quenching process with water, and also release of nitrogen. SETs with air oxidation under oxygen starvation conditions also showed presence of zirconium nitride in the post-test examination [14,15]. The Sandia Fuel experiments showed strong nitrogen uptake during the oxygen starvation stage of the experiments and nitrogen release during re-oxidation of the zirconium nitride later on [16]. Not all those behaviours could be calculated with severe accident codes, because models for the nitrogen/nitride reactions were limited, e.g. ATHLET-CD and SOCRAT, or unavailable, e.g. MELCOR and SCDAP. PSI, Switzerland, and KIT, Germany, launched a project for the development of a computer model to describe the nitrogen as direct reaction partner in the oxidation of zirconium based cladding materials.

Due to the slower nitriding process compared with oxidation, the new model is most important when the temperature increases slowly, e.g. accidents where the nuclear heating is low enough that the escalation is largely driven by the chemical reactions. Those types of scenarios are most typical following an accident in spent fuel pools or wet storage pools, where the environment will include any or all of steam, oxygen and nitrogen. An accident in a spent fuel pool following total loss of coolant can lead to high temperatures and severe degradation of the fuel, opening ready pathways for major releases of volatile fission products. Moreover, reactions between oxygen and exposed overheated fuel can render some fission products in a more volatile state. The Sandia fuel experiments showed that once all the coolant is lost, the highly energetic zirconium-oxidation reaction in air and following sustained nitriding, can bring about such an escalation within half a day.

The present nitriding work followed on from work performed at PSI to specifically address nitrogen promoted oxidation in air from which models for oxidation in air had been developed and implemented into SCDAPSim/PSI, MELCOR 1.8.6/PSI, and standard MELCOR 2.x. The PSI air oxidation model [17] was designed to model both breakaway in steam at temperatures below 1050 °C and oxidation in air. It is based on the observed phenomenon in which nitrogen degrades the protective character of the oxide layer in a way that has a similar macroscopic effect as breakaway oxidation, inducing a transition from parabolic to quasi-linear kinetics. The nitride layer is observed to be similarly non-protective [7]. Parallel developments were performed by GRS and EDF, and implemented into ATHLET-CD [18] and MAAP, respectively [19]. More recently a model for nitriding was developed and introduced into ATHLET-CD [18]. At this stage no released code version included a model for oxidation of ZrN.

The purpose of the present study was to extend the capability of the PSI air oxidation model to include both the formation and oxidation of nitride. It is noted that cladding oxidation and nitriding in air are dominant issues in a spent fuel accident, since the decay heat levels are low and the fuel is likely to undergo slow heating and long periods of time (if cooling is not restored) at temperatures in the breakaway regime.

The present nitriding project comprised two steps. The first step was to conduct separate-effects tests in the frame of a PhD thesis [20] to produce a database for the kinetics of the oxidation, nitriding, nitride oxidation reactions, together with compositional data from post-test examinations. The second step was to construct and assess a computer model for the reactions, incorporate the kinetic parameters derived from the database, for inclusion in severe accident codes. The model development and implementation part of the second step is complete, while the assessment is in progress at this time.

The following sections describe the model for the Zr-air-steam reactions: its physical basis, the reaction scheme and kinetics, the model phases, implementation in the severe accident code MELCOR, illustrative comparison results with SETs data results, and finally summarises its present status.

2. Phenomenology

2.1. Physical basis

Earlier SETs performed at KIT essentially aimed at investigating oxidation of Zr-based cladding in air and other nitrogen containing atmospheres, showed that although nitrogen reacts very slowly with metallic Zr, it reacts fairly rapidly with oxygen-stabilised α-Zr(O) which is a metallic phase with absorbed oxygen, and with sub-stoichiometric oxide [7,21]. The more recent SETs performed by Park [20] specifically targeted the pre-oxidation (PO) - nitriding (NT) - re-oxidation (RO) phases in the sequence in order to provide sufficient data to develop a workable model. To effectively separate the different reactions taking place under different gas atmospheres, and the effect of different gas mixtures on the reactions, the tests were carried out in three sequential stages: pre-oxidation in oxygen, nitriding in nitrogen and re-oxidation in oxygen. A carrier gas of argon was used in all stages. For practical reasons, no steam could be used in any of the tests, therefore oxygen was used as a surrogate.

The SETs were performed using 10 mm long samples of Zircaloy-4 in four series at different temperatures: 900, 1000, 1100, and 1200 °C, with a range of time durations for the PO and NT phases. In addition, some of the tests were repeated with termination at intermediate times during NT to allow inspections to determine the micromorphology and composition prior to RO. Two different experimental thermo-balance set-ups were used for the tests, Netzsch STA and Setaram TAG (see Fig. 1).

Transient data were obtained for the gross mass gain from the combined uptake of oxygen during PO, the nitrogen during NT, and the balance of oxygen uptake and nitrogen release during RO. In principle, the three separate phases should definitely determine the separate contributions, but there were transition periods between PO and NT and between NT and RO when the reaction chamber contained a mixture of different gases, and the contributions were uncertain. Although the transition periods made the kinetic quantification less precise, they could not be prevented without including phases of inert gas flow to allow the former reaction gas to be purged from the chamber, which would have made the test conditions less representative. In a real accident sequence, there would be mixtures of reacting gases for at least part of the time. The uncertainties could not be eliminated, but were reduced by analyses made on the basis of gas exchange time in the chamber, the observed changes in the mass gain rates, post-test determinations of the

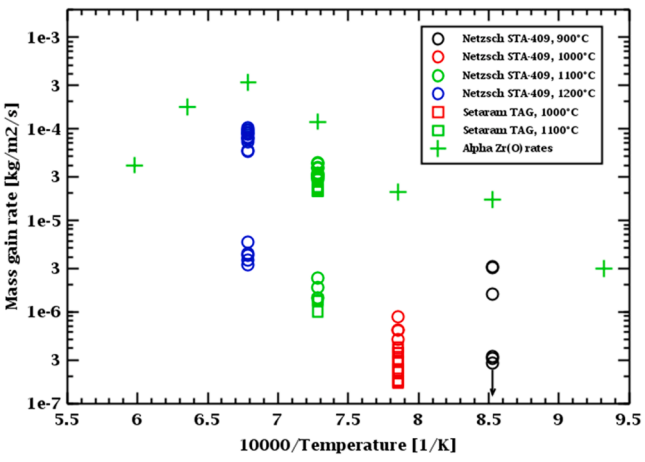

Fig. 1. Reaction rates for fast and slow nitriding of zircaloy cladding [20] and pure α Zr(O) [17].

final Zr, α-Zr(O), ZrO_2 and ZrN fractions, and the overall mass gain.

2.2. Summary of findings

The findings from the test program reveal a complex phenomenology, described below [20,22].

Pre-oxidation: The PO comprised an initial short period of rapid mass gain, with complete oxygen consumption in some cases, before the rate declined and became limited by the kinetics of the diffusion of oxygen across the growing oxide layer.

Both ZrO_2 and α-Zr(O) were formed during PO. The fractions of formed ZrO_2 and α-Zr(O) could not be determined based on the tests.

The oxidation kinetics were generally parabolic after an initial starvation period. However, longer (60 min) PO cases at 900 °C and 1000 °C exhibited an acceleration due to transition to breakaway oxidation.

The mass gain continued at about the same rate during the PO to NT transition, before the residual, non-consumed oxygen was purged, and in some cases temporarily increased due to the effect of nitrogen on the oxidation kinetics.

The formation of α-Zr(O) took place at all temperatures studied, but was much more extensive at 1100 and 1200 °C than at 900 and 1000 °C. As a consequence, the greater α-Zr(O) at the higher temperatures lead to proportionally greater ZrN production once nitriding started. It is thought that the main reason is the transition from monoclinic to tetragonal oxide microstructure at ca. 1050 C, allowing the oxygen to diffuse much more readily through the oxide scale.

Nitriding: The nitriding mass gain qualitatively correlates with the α-Zr(O) availability. Fig. 1 shows that the total mass gain measured in the present series of SETs exhibits a dependence on temperature that qualitatively correlates with the production of α-Zr(O), the latter determined from post-test inspection of oxidised samples from a separate series of SETs performed at KIT. Quantitative significance cannot be deduced, since the present results for each temperature cover a range of reaction durations in two different experimental devices (STA and TAG). The results from a separate set of tests also show a maximum α-Zr(O) production rate at ca. 1400 °C. Complementary SETs at KIT on the reaction of ZrO_x with nitrogen show an analogous trend in the temperature dependence of the ZrN formation [23].

Fig. 2 shows a segment of a sample after PO and NT at 1100 °C. The ZrN (yellow/gold) is almost all located at the outer surface and just underneath the oxide, with some also along radial cracks in the oxide. It was at these locations where the α-Zr(O) was observed in other oxidation + annealing tests at KIT [24]. One would expect the Zr(N) to be predominantly where the α-Zr(O) had formed, which is according to the phase diagram at the metal/oxide interface and, under starvation conditions also at the oxide surface, as described by Stuckert [24].

Fig. 3 shows a vertical cut through a specimen of a SET with 10 min of pre-oxidation in oxygen and 1 hour of nitriding at 1100 °C, further illustrating the stochastic nature of the reaction phenomena. On the right side (inner surface), the zirconium nitride (gold) has not broken through the underlying oxide layer (grey), and the layers are essentially coherent. Therefore no nitriding reaction of the α-Zr(O) between oxide layer and metal occurred.

On the left side (outer surface), the nitriding reaction penetrated through the oxide layer and has started to react with the underlying α-Zr (O). Here, the arrangements of both the nitride and oxide exhibit partially connected patches of one within the other. The reason for the more advanced nitriding and quite different topology may be the cracks that formed through the oxide during PO, and then became sites for nitride to form during NT. It is conjectured that the outer oxide is more susceptible to becoming cracked due to tensile hoop stresses, while the inner surface layer was in compressive stress.

Following transition to nitriding, there was a period of fairly rapid mass gain, as the α-Zr(O) readily converted to ZrN. During tests with a long NT period, all the α- Zr(O) was converted to ZrN and ZrO_2, leaving only the β-Zr to react. The mass gain then dropped to a much lower (ca. 1/20) rate. In a few long NT cases the mass gain stopped, as all of the initial Zr had reacted to form oxide and nitride. These cases were valuable in helping to quantify the final separate masses, and hence reduce the uncertainties due to the transition period.

The nitriding kinetics was essentially linear, indicating the nitride layer which was formed was non-protective against continuing reaction.

Re-oxidation: During RO, the ZrN was oxidised rapidly leading to oxygen starvation in the higher temperature cases. In some cases, all the nitride was converted to oxide. The oxidation of the remaining Zr/ α-Zr (O) continued, though at a slower rate than oxidation of the ZrN.

Like the nitriding, the ZrN oxidation kinetics were essentially linear, due to the non-protective nature of the oxide thus formed. It is noted that ZrN is a very dense material, resulting in a local volume reduction in the vicinity of the lower density of ZrO_2. This leads to breakaway-like behaviour of the oxide/nitride layer at all temperatures, including above 1050 °C where breakaway oxidation in steam does not occur.

During RO, the ZrN previously formed during NT appeared to have been rapidly and extensively oxidised, so that a large fraction of the reacted part of the sample was oxide. However, it cannot definitely be determined to what extent the ZrN was oxidised before Zr/ α-Zr(O) oxidation occurred. There was likely to have been some period when

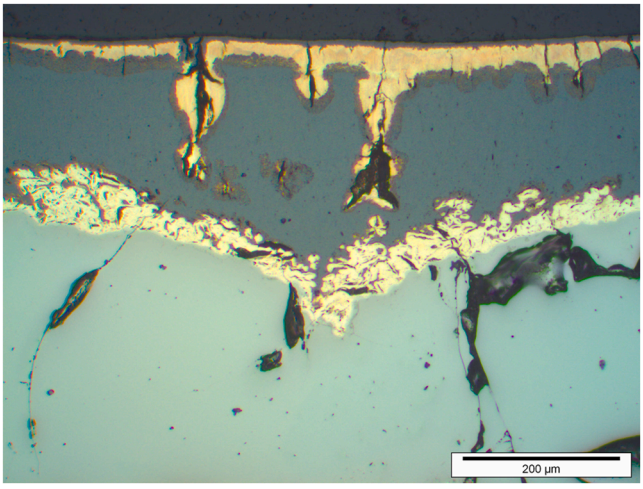

Fig. 2. ZrN with oxide ingots at 1100 °C experiment with pre-oxidation and nitriding. The black areas in the micrograph are voids presumably created during sample preparation.

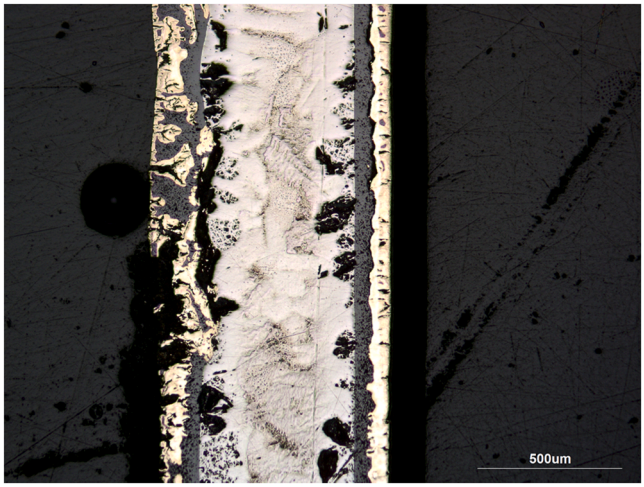

Fig. 3. Zircaloy tube at 1100 °C, 10 min pre-oxidation and 1 h nitriding.

both ZrN and Zr metal were oxidised. Inspection of the samples showed some remaining ZrN.

There are signs that the Zr/ α-Zr(O) oxidation kinetics were linear during RO, but due to the highly compromised state of the samples, that cannot be definitely determined.

These findings are used as the basis for the model described below.

Significance of α-Zr(O): The α-Zr(O) is an important quantity for controlling the nitride formation. However, since it was not possible to directly determine kinetic data on its formation, use is made of standard correlations, beneath which the production of α-Zr(O) by diffusion of oxygen from the oxide layer to the metal is included. The SETs data for mass gain during nitriding show a first period of fairly rapid ZrN formation, attributed to the nitriding of α-Zr(O), followed by a period of much slower ZrN formation, attributed to the nitriding of metallic Zr. The nitriding of α-Zr(O) and metallic are separately represented during the (oxidant-starved) nitriding period. Also included are the oxidation of α-Zr(O) and ZrN during re-oxidation, with kinetics based, again, on the SET data. Instead of one oxidation process, the new model includes five different chemical processes for the interaction of the atmosphere with zirconium based cladding materials.

3. Description of model

Reaction precedence: The following reaction precedence is assumed throughout the model: oxidation by oxygen > oxidation by steam > nitriding. Even though this is supported by both empirical observations and basic thermodynamic data, the oxidation mechanism is in reality more complex and determined by the local conditions, i.e., at the metal/ oxide and oxide/gas interfaces.

3.1. Model philosophy

The new nitriding model extends the number of chemically active species to include nitrogen (hitherto treated as a catalyst for the oxidation), and ZrN. An auxiliary species is the oxygen-stabilised alpha-zirconium which we refer to α-Zr(O) and, as mentioned above, readily reacts with nitrogen forming ZrN under oxygen-starved conditions. Consequently, four different zirconium species, metal, oxide, α-Zr(O), and nitride are reaction partners for three gases in the atmosphere, oxygen, steam and nitrogen.

It may be helpful to remark of the nature of alpha-zirconium, with or without dissolved oxygen. Alpha-zirconium is the low-temperature phase of Zr, which converts to the high-temperature beta phase at 860 °C. At high temperatures beyond 860 °C, it can be stabilized by oxygen (and nitrogen) initially produced by diffusion of oxygen from the ambient atmosphere and, after formation of a protective zirconium oxide layer from the oxide to the metal. The oxygen concentration of α-Zr(O) can vary up to the saturation level, which is temperature dependant and typically about 7 percent by mass. Within the partially oxidised cladding, the concentration is at saturation at the oxide-metal interface and decreases through the underlying metal. Diffusion of oxygen from the oxide takes place down the concentration gradient. In the computer model, a simplifying assumption is made in that the content of oxygen in the α-Zr(O) is set to 6.5 wt% of the zirconium weight, which is the maximum percentage of the oxygen found in the α-Zr(O) layer [25] and is close to equilibrium.

This representation of the oxidation/nitriding processes is necessarily simplified. There is some evidence that during nitriding, ternary species such as Zr-oxynitrides are formed, perhaps as metastable intermediary species [20]. It is also not possible to deduce from the data the extent to which residual α-Zr(O) is converted to ZrO2 during the nitriding of α-Zr(O). There are other simplifications implicit in the reaction scheme described below, to deal with the complex and stochastic nature of the processes discussed in the previous section, and to address programming and numerical related issues.

The nitriding kinetics in the model are based on the layer thicknesses model of the different zirconium species in a way analogous to the PSI breakaway and air oxidation model [17] where the non-protective nature of the oxide and nitride layers are represented by using, for the kinetics, an effective thickness less than the physical thickness.

The additional species added to the nitriding model multiplies the number of possible chemical reactions as compared to the PSI breakaway and air oxidation model, some of which may be competing with each other. A strategy is formulated to represent the precedence amongst the group of reactions.

3.2. Reaction scheme and kinetics

Four different zirconium species, metallic (β-Zr), oxide (ZrO_2), metallic alpha-zirconium (α-Zr(O)) and nitride (ZrN) are reaction partners for three gases in the atmosphere, oxygen, steam and nitrogen. The consumption of the solid material layers due to reaction with gas species is multiplied with a transition factor, when the layer thickness is below 30 μm. This transition factor prevents sharp changes of reaction rates in case of a complete consumption of a layer. Depending on the availability of the reacting gases, several different reactions can occur in parallel, e. g. nitriding, oxidation and alpha layer production under partial oxidant starvation conditions. In all combinations of gas presence and material layer presence, the mass conservation is fulfilled in the nitriding model. In 45 different combinations of gases and material layers the nitriding model is calculating the production of α-Zr(O), zirconium oxide and zirconium nitride. All three phases can be produced, but also consumed: α-Zr(O) by oxidation and nitriding, zirconium oxide by diffusion, and zirconium nitride by oxidation.

A comparatively large number of chemical reactions and transport processes involving species in the gas phase – H_2O, O_2, N_2, H_2 – and the cladding media – Zr, α-Zr(O), ZrN, ZrO_2. These are represented in a simplified way in the following.

3.3. Reaction processes for zr and α-Zr(O)

In the presence of oxygen:

$$Zr + (0.8x+0.2)\ O_2 = x\ ZrO_2 + (1\text{-}x)\ ZrO_{0.4}. \quad (1)$$

In which x is the fraction of ZrO_2 formed in the reaction, and (1-x) if the fraction α-Zr(O).

In the presence of steam and absence of oxygen:

$$Zr + (1.6x+0.4)\ H_2O = x\ ZrO_2 + (1\text{-}x)\ ZrO_{0.4} + (1.6 + 0.4)\ H_2. \quad (2)$$

For production of ZrO_2 in steam, the Cathcart-Pawel correlation is used for mass gain rate WG_{Rate} in kg/m^2/s:

$$WG_{Rate} = 36.2\ \times e^{\left(\frac{-20\_111}{T}\right)} \Big/ (2\ \times c1\ \times th), T < 1853\text{K} \quad (Ia)$$

$$WG_{Rate} = 10.117\ \times e^{\left(\frac{-16\_610}{T}\right)} \Big/ (2\ \times c1\ \times th), T > 1873\text{K} \quad (Ib)$$

and linearly interpolated at $1853 < T < 1873$.

Here *th* is the oxide thickness and *c1* is the density of ZrO_2 multiplied by the mass gain ratio, {M(ZrO_2) – M(Zr)}/M(Zr) = ca.0.26. In the event of breakaway, an effective thickness, th_{eff}, is used as described in [13].

The parabolic dependence:

$$\frac{d(th)^2}{dt} = f(T) \quad (II)$$

is recast in the form:

$$\frac{d(th)}{dt} = \frac{f(T)}{2\ \times th} \quad (III)$$

Diffusion occurs during oxidation itself, and is included in most of the oxidation weight gain correlations [25], and continues after the end of oxidation without changing the weight. The diffusion does not take place if a ZrN layer exists between the oxide and the metal or if breakaway has been induced at temperatures below 1050 °C. In the case of breakaway, oxygen can access the underlying metal directly, resulting in faster production of oxide, which is taken into account in the air-oxidation and breakaway model [17].

The formation of α-Zr(O) starts simultaneously with the oxidation process. If the oxidant flow rate calculated by the code based on initial boundary conditions is smaller than the calculated diffusion rate, the production of alpha layer is flow rate limited. Otherwise, the alpha production mass gain rate is subtracted from the oxide mass gain rate. In the absence of a clear understanding of how best to use existing empirical correlations to treat the interacting processes of diffusion and chemical reaction, an ad-hoc approach is adopted as an interim measure to calculate the α-Zr(O) formation. The kinetic expressions are adapted from an existing correlation in such a way as to provide an acceptable fit to data from annealing tests [26]. The diffusion rate does not depend on the oxide layer thickness if the oxide layer is thicker than 30 μm and so the following temperature dependant rate law [25] is used in the model:

$$WG_{Rate}(T) = 278.8 \times e^{\frac{-24\_227}{T}},\ T < 2073\text{K} \quad \text{(IVa)}$$

$$WG_{Rate}(T) = 0.09422 \times e^{\frac{-10\_252}{T}},\ T > 2173 \quad \text{(IVb)}$$

and interpolated between 2073 and 2173 K.

It is noted that the production of α-Zr(O) continues via diffusion from the oxide, even if oxygen is no longer present in the flowing gas.

We treat reaction (II) as though it is a single process. The molecular bonds are broken at the surface of the growing oxide layer, and the oxygen atoms diffuse through the oxide to react at the interface with the underlying Zr (or α-Zr(O)). The solid state processes are essentially the same for oxidation by steam and oxygen, except when the oxide layer is damaged, when gaseous hydrogen can penetrate and accumulate in the cracks and pores. However, the gas transport is somewhat affected by the hydrogen or other non-condensable gases, while the energy needed to break the molecular bonds is greater for steam than oxygen, per mole of Zr oxidised. The empirical data for the respective oxidation kinetics, and hence the correlations, may be slightly different as a result. We also note that the precedence (oxygen > steam) stems from the gas phase chemistry. If steam were consumed in the presence of oxygen, the released hydrogen would rapidly combine with the remaining oxygen to recover the steam consumed.

For practical purposes, in the model we assume all the oxide is ZrO_2, and all the α-Zr(O) has an oxygen fraction of 6.5% w/w, which is close to saturation and almost exactly equivalent to $ZrO_{0.4}$. In reality, the average fraction may be higher or lower, and there is typically an oxygen concentration gradient across both the cladding and the oxide.

Under non-starved oxidant conditions, the α-Zr(O) fraction, x, is determined by the kinetic correlations for oxide and α-Zr(O) formation. However, the α-Zr(O) is formed by diffusion of oxygen into the underlying metallic Zr and continues even if there is no oxidant available in the gas. The correlation for α-Zr(O) formation is recast in diffusion form in order to capture this.

In the presence of nitrogen and absence of both oxygen and steam:

$$2ZrO_{0.4} + N_2 = 2ZrN + 0.8[O] \quad (3)$$

$$ZrO_{0.4} + 1.6[O] = ZrO_2 \quad (4a)$$

$$Zr + 2[O] = ZrO_2 \quad (4b)$$

$$2Zr + N_2 = 2ZrN \quad (5)$$

The kinetics for the fast nitriding of α-Zr(O) (3) and slow nitriding of Zr (5) are both linear, and correlate with the SETs data as, respectively:

$$WG_{Rate}(T) = 213.88 \times e^{\frac{-22\_087}{T}} \quad \text{(Va)}$$

$$WG_{Rate}(T) = 110.0 \times e^{\frac{-25\_000}{T}} \quad \text{(Vb)}$$

Reactions (4a, b) are assumed to follow immediately from (3), so that oxygen is retained within the cladding medium during nitriding. It is also assumed that the second reaction (4a) takes precedence over the third (4b), i.e. residual α-Zr(O) is converted to ZrO_2 before further α-Zr (O) is formed. Eqs. (3) and (4) imply recovery of 4 out of 5 mol of α-Zr(O) reacted; therefore the nitriding process only slowly depletes the α-Zr(O) inventory.

It is also assumed that the nitriding of α-Zr(O) (3) takes precedence over that of metallic Zr (5), so that reaction (5) takes place only after all the α-Zr(O) is converted to ZrN. The nitriding stops when no Zr remains.

3.4. Oxidation of ZrN

In the presence of oxygen or steam:

$$2ZrN + 2O_2 = 2ZrO_2 + N_2 \quad (6)$$

$$2ZrN + 4H_2O = 2ZrO_2 + N_2 + 4H_2 \quad (7)$$

All the nitrogen produced by (6) and (7) is released from the reacted cladding medium. In the model, the nitrogen released from the re-oxidation is added into the corresponding volume and can be used for nitriding reaction in the following nodes.

The kinetics are inherently uncertain due to the fact that the ZrN may be distributed within the cladding in many different ways – externally or internally with respect to the oxide, or embedded within the metallic Zr, α-Zr(O), or ZrO_2, or any combination of these locations. The data show that the oxidation is much more rapid than would be estimated by any of the parabolic correlations used in conjunction with any thickness that might correspond to the quantity of previously formed ZrO_2/ZrN. It is clear that there is little resistance to the transport of oxidant to the nitride, and the resistance does not noticeably increase as the reaction proceeds. The kinetic behaviour is typical of the fully transitioned pseudo-breakaway oxidation in air, which might be expected in view of the loss of structural coherence of the oxide caused by nitride embedded within the oxide.

From the SETs data, the kinetics of ZrN oxidation are reasonably well approximated by four times the same Cathcart-Pawel correlation as used during PO, but with an effective oxide thickness corresponding to pseudo-breakaway oxidation resulting from the non-protective nature of the reacted layer following nitriding.

The rate of ZrN oxidation used in the model is

$$WG_{Rate}(T) = 144.8 \times e^{\left(\frac{-20\_111}{T}\right)} \Big/ \left(2 \times c1 \times th_{eff}\right) \quad \text{(VI)}$$

where th_{eff} is the effective oxide thickness in the air-oxidation pseudo-breakaway model [17].

4. Model comparison with selected set data

Sample calculations with the PSI version of MELCOR 1.8.6/NT illustrate the way modelled processes affect the oxidation and nitriding phenomena.

Figs. 4 and 5 compare the modelled and observed thickness of the oxide layer after 20 min (1000 °C) and 10 min (1100 °C) oxidation in oxygen followed by 3 h and 6 h of annealing in argon at 1000 and 1100 °C. These tests were conducted to separately investigate the thinning of the ZrO_2 scale by oxygen diffusion into the metal phase forming α-Zr(O), and thereby contained no nitrogen. As can be seen, the thickness ofthe oxide layer after oxidation decreases as more and more of the oxygen diffuses into the underlying Zr forming metallic α-Zr(O).

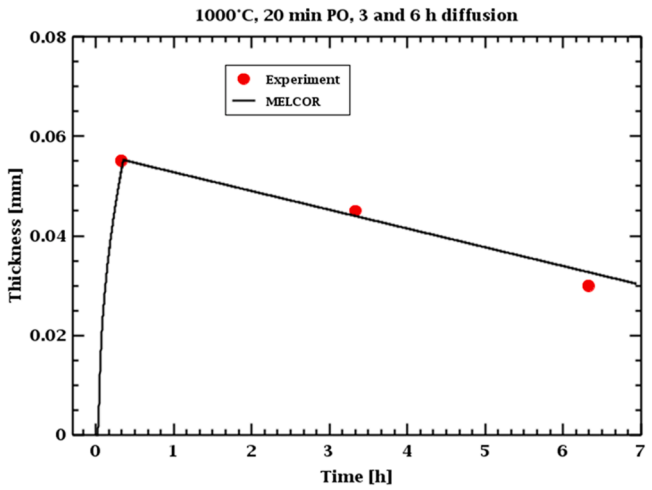

Fig. 4. Oxide layer growth at 1000 °C with following diffusion of oxygen to Zr-metal.

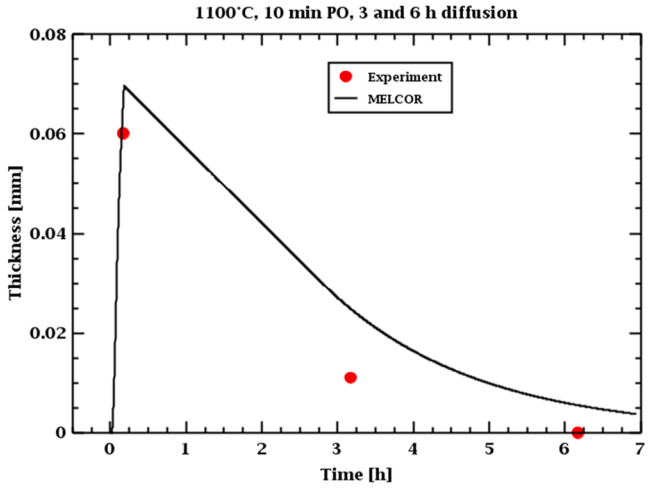

Fig. 5. Oxide layer growth at 1100 °C with following diffusion of oxygen to Zr-metal.

The dissolution of oxygen in the Zr metal is much faster at 1100 °C than at 1000 °C, with a result, which may explain the much more extensive nitriding observed in the tests themselves. Complete conversion to saturated α-Zr(O) could be achieved by homogenizing an oxide layer of depth ca. 0.07 mm uniformly on both inner and outer surfaces.

In Fig. 6, the results of a MELCOR calculation for a separate-effects test at 1100 °C is shown with the measured weight gain of several tests. The different tests were conducted with 10 min of pre-oxidation, 0.5, 1.0, 3.0, 6.0 and 15 h of nitriding and one test with 20 min of re-oxidation after 15 h of nitriding. The time profiles for the mass gain show clearly the respective reactions: the oxide formation during PO, the fast and slow nitriding of the α-Zr(O) and metallic Zr, and the rapid oxidation of nitride, in both the test and calculation, showing excellent qualitative agreement. Quantitatively, the pre-oxidation as well as the fast and slow nitriding mechanisms are in reasonably good agreement with the experimental data bearing in mind the stochastic nature of the mechanical behaviour of the cladding materials and hence its impact on the observed reaction phenomena. This is shown clearly from the case-to-case differences in the experimental data, e.g., Fig. 6, as well as from the post-test examinations discussed previously, see Figs. 2 and 3, despite the identical boundary conditions until the test has been finished. Comparison with data for the single case with re-oxidation shows an underestimation in re-oxidation mass gain, but the observed

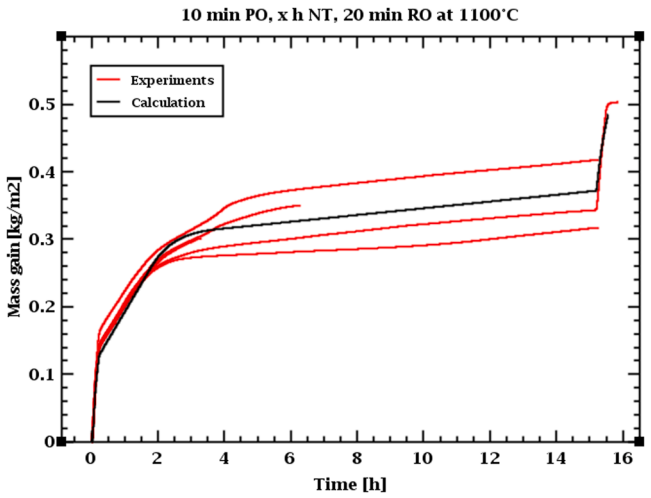

Fig. 6. Weight gain data of experiments at 1100 °C with MELCOR calculation.

case to case variations suggest that caution should be used in attaching quantitative significance.

4.1. Summary and conclusions

Results of separate-effects experiments at KIT have been used to identify, during an air ingress sequence, the reaction chain comprising oxidation, nitriding, and re-oxidation.

The key elements of the reaction chain are: (1) formation of α-Zr(O) during and following oxidation; (2) reaction between the α-Zr(O) and nitrogen to produce non-protective nitride layer; (3) re-oxidation of the nitride and remaining Zr/α-Zr(O), with the release of nitrogen.

The experimental data enabled quantification of the kinetics of the reactions steps, which was used in a predictive model. The model was implemented in MELCOR 1.8.6 (3084) PSI code version.

The MELCOR code version will enable the code to simulate reactor and SFP air ingress sequences and air/steam mixtures involving periods of oxidant starvation.

In a first stage of assessment, the model is shown to successfully reproduce the reaction phenomena sequence, and give good agreement for the measured compositional signatures, namely α-Zr(O), ZrO_2 and ZrN masses.

Assessment against air ingress integral experiments with oxidant starvation is in progress, commencing with QUENCH-16. It is foreseen to continue with further experiments, such as QUENCH-18 and the Sandia Fuel Project, Phase I and Phase II.

CRediT authorship contribution statement

B.S. Jäckel: Investigation, Writing – original draft. **J.C. Birchley:** Investigation, Formal analysis, Writing – original draft. **T. Lind:** Investigation, Writing – review & editing. **M. Steinbrück:** Writing – review & editing. **S. Park:** Investigation, Writing – review & editing.

Declaration of Competing Interest

The authors declare that they have no known competing financial interests or personal relationships that could have appeared to influence the work reported in this paper.

Data availability

Data will be made available on request.

Acknowledgements

The project was financially supported by the Swiss Federal Nuclear Safety Inspectorate ENSI under contract CTR00321(2017–2021). Two of the main authors are retired and have voluntarily dedicated their time to prepare this manuscript which is gratefully acknowledged.

References

[1] Powers, D., Kmetyk, L., Schmidt, R. (1994). A review of technical issues of air ingression during severe reactor accidents. Sandia National Lab., Report NUREG/CR-6218, SAND94-0731, Sandia National Lab., 1994.
[2] J.R. Wolf, J.L. Rempe, L.A. Stickler, G.E. Korth, D.R. Diercks, L.A. Neimark, D. W. Akers, B.K. Schuetz, T.L. Shearer, S.A. Chdvez, G.L. Thinnes, R.J. Witt, M. L. Corradini, J.A. Kos, TMI-2 Vessel Investigation Project Integration Report, NUREG/CR-6197, Idaho National Engineering Laboratory, 1993.
[3] K. Natesan, W.K. Soppet, S. Basu, in: Low Temperature Air Oxidation Experiments at ANL, CSARP Meeting, Crystal City, VA, 2004.
[4] Z. Hózer, E. Szabó, T. Pintér, I. Varjú, T. Bujtás, G. Farkas, N. Vajda, Activity release from damaged fuel during the Paks-2 cleaning tank incident in the spent fuel storage pool, J. Nucl. Mater. 392 (2009) 90–94, https://doi.org/10.1016/j.jnucmat.2009.03.049.
[5] C. Duriez, T. Dupont, B. Schmet, F. Enoch, Zircaloy-4 and M5® high temperature oxidation and nitriding in air, J. Nucl. Mater. 380 (2008) 30–45, https://doi.org/10.1016/j.jnucmat.2008.07.002.
[6] M. Steinbrück, A. Miassoedov, G. Schanz, L. Sepold, U. Stegmaier, J. Stuckert, Experiments on air ingress during severe accidents in LWRs, Nucl. Eng. Des. 236 (2006) 1709–1719, https://doi.org/10.1016/j.nucengdes.2006.04.010.
[7] M. Steinbrück, Prototypical experiments relating to air oxidation of Zircaloy-4 at high temperatures, J. Nucl. Mater. 392 (2009) 531–544, https://doi.org/10.1016/j.jnucmat.2009.04.018.
[8] M. Steinbrück, M. Grosse, L. Sepold, J. Stuckert, Synopsis and outcome of the QUENCH experimental program, Nucl. Eng. Design 240 (2010) 1714–1727, https://doi.org/10.1016/j.nucengdes.2010.03.021.
[9] L. Fernandez-Moguel, J. Birchley, Simulation of air oxidation during a reactor accident sequence: part 2 – Analysis of PARAMETER-SF4 air ingress experiment using RELAP5/SCDAPSIM, Ann. Nucl. Energy 40 (2012) 141–152, https://doi.org/10.1016/j.anucene.2011.10.018.
[10] Z. Hozer, P. Windberg, I. Nagy, L. Maroti, L. Matus, M. Horvath, A. Pinter Csordas, M. Balasko, A. Czitrovszky, P. Jani, Interaction of Failed Fuel Rods Under Air Ingress Conditions, Nucl. Technol. 141 (2017) 244–256, https://doi.org/10.13182/NT03-A3365.
[11] M. Adorni, L.E. Herranz, T. Hollands, K.-I. Ahn, C. Bals, F. D'Auria, G.L. Horvath, B. S. Jaeckel, H.-C. Kim, J.-J. Lee, M. Ogino, Z. Techy, A. Velazquez-Lozad, A. Zigh, R. Rehacek, OECD/NEA Sandia Fuel Project phase I: benchmark of the ignition testing, Nucl. Eng. Design 307 (2016) 418–430, https://doi.org/10.1016/j.nucengdes.2016.07.016.
[12] J. Stuckert, M. Steinbrück, Experimental results of the QUENCH-16 bundle test on air ingress, Prog. Nucl. Energy 71 (2014) 134–141, https://doi.org/10.1016/j.pnucene.2013.12.001.
[13] J. Stuckert, M. Steinbrueck, J. Kalilainen, T. Lind, J. Birchley, Experimental and modelling results of the QUENCH-18 bundle experiment on air ingress, cladding melting and aerosol release, Nucl. Eng. Des. 379 (2021), https://doi.org/10.1016/j.nucengdes.2021.111267.
[14] M. Steinbrück, M. Böttcher, Air oxidation of Zircaloy-4, M5® and ZIRLO™ cladding alloys at high temperatures, J. Nucl. Mater. 414 (2011) 276–285, https://doi.org/10.1016/j.jnucmat.2011.04.012.
[15] M. Steinbrück, S. Schaffer, High-Temperature Oxidation of Zircaloy-4 in Oxygen–Nitrogen Mixtures, Oxid. Met. 85 (2015) 245–262, https://doi.org/10.1007/s11085-015-9572-1.
[16] Zigh, A., Velazquez-Lozada, A. (2014). OECD-NEA Sandia Fuel Project (SFP). Retrieved from http://www.oecd-nea.org/jointproj/sfp.html.
[17] J. Birchley, L. Fernandez-Moguel, Simulation of air oxidation during a reactor accident sequence: part 1 - Phenomenology and model development, Ann. Nucl. Energy 40 (2012) 163–170, https://doi.org/10.1016/j.anucene.2011.10.019.
[18] A. Wielenberg, L. Lovasz, P. Pandazis, A. Papukchiev, L. Tiborcz, P.J. Schöffel, C. Spengler, M. Sonnenkalb, A. Schaffrath, Recent improvements in the system code package AC2 2019 for the safety analysis of nuclear reactors, Nucl. Eng. Design 110211 (2019), https://doi.org/10.1016/j.nucengdes.2019.110211.
[19] M.F. Haurais, Evaluate the contribution of the fuel cladding oxidation process on the hydrogen production from the reflooding during a potential severe accident in a nuclear reactor, PhD thesis, l'Université Paris-Saclay, 2016.
[20] S. Park, Nitriding and *Re*-oxidation Behavior of Zircaloy-4 At High Temperatures PhD Thesis, ETH Zürich, 2020, https://doi.org/10.3929/ethz-b-000459694. No. 27146.
[21] M. Steinbrück, High-temperature reaction of oxygen-stabilized α-Zr(O) with nitrogen, J. Nucl. Mater. 447 (2014) 46–55, https://doi.org/10.1016/j.jnucmat.2013.12.024.
[22] S. Park, T. Lind, J. Birchley, M. Steinbrueck, Current understanding of high-temperature oxidation phenomena during air ingress scenarios, in: Proceedings of the 10th European Review Meeting on Severe Accident Research (ERMSAR2022), Karlsruhe, Germany, 2022.
[23] M. Steinbrück, S. Prestel, U. Gerhards, High-temperature interaction of oxygen-preloaded Zr1Nb alloy with nitrogen, Nuclear. Engineering. and. Technology 50 (2018) 237–245, https://doi.org/10.1016/j.net.2017.12.017.
[24] J. Stuckert, M.S. Veshchunov, Behaviour of Oxide Layer of Zirconium-Based Fuel Rod Cladding Under Steam Starvation Conditions, Forschungszentrum Karlsruhe, Karlsruhe, Germany, 2008, https://doi.org/10.5445/IR/270071587.
[25] G. Schanz, B. Adroguer, A. Volchek, Advanced treatment of zircaloy cladding high-temperature oxidation in severe accident code calculations Part I. Experimental database and basic modeling, Nucl. Eng. Des. 232 (2004) 75–84, https://doi.org/10.1016/j.nucengdes.2004.02.013.
[26] R. Pawel, J. Cathcart, R. McKee, The Kinetics of Oxidation of Zircaloy-4 in Steam at High Temperatures, J. Electrochem. Soc 126 (1979) 1105–1111.